International Journal of Science and Research (IJSR)
ISSN: 2319-7064
Impact Factor 2025: 7.089

Mitigating UV Effect on Space Materials by Cobalt Doped Stannic Dioxide Nanocrystal Coat

Monalisa

M. Tech. in Nanoscience and Nanotechnology, AK University, Ph.D. scholar, NIT, Patna

Abstract: ***Materials deployed in outer space are subject to harsh and unfiltered solar radiation and cosmic rays. Vacuum ultraviolet rays and cosmic rays severely degrade conventional optical components. Solarization and lattice displacement being major issues, this study investigates possible mitigation of hazards by space ultraviolet compatibility and optical radiation behaviour of cobalt-doped stannic dioxide nanocrystals synthesized using facile co-precipitation green route. UV-Visible absorption reveals systematic behaviour in band structural, microstructural and properties of optical conductivity, optical density, refractive index, extinction coefficients, and absorbance prominently in UV region. Several effects such radiation blocking and solarization are governed by 3d states and mid-gap levels. Cobalt doping effectively suppressed formation of radiation induced colour centres by mitigating structural disorder. Moreover, the nano-size morphology provides high surface-to-volume ratio which facilitates rapid dynamic relaxation (likely, self-healing) of lattice strains. The features establish the materials synthesized and studied as a highly viable candidate for transparent conductive oxide coatings, space-grade solar cell protective windows and deep-space optoelectronic sensors.***

Keywords: optical absorption, cobalt-doped stannic dioxide nanoparticles, space materials, vacuum UV, solarization resistance, radiation hardened materials.

1. Introduction

Aerospace hardware is exposed to incredibly hostile environment characterized by extreme vacuum pressure of interstellar regions, thermal cycling, and intense radiation fields. Among the environmental hazards, sun's radiation in the range of 100 nm to 200 nm is especially damaging, and is critical threat to the operational longevity of space craft components and software. As there is no ozone layer around, the vacuum UV photons attack outer structure, optical windows, and solar arrays continuously [1].

To tackle the catastrophic material degradation, conventional transparent conductive oxides and glass cover are used widely. Solar cells and sensor windows exposed to prolonged radiation undergo a damage called solarization. High energy photons, in the process, excite electrons in materials and causes trapping, particularly in naturally occurring lattice defects. This creates light-absorption, optical darkening, transmission loss, and, over time, reduced efficiency. Furthermore, materials get brittle and structurally compromised.

It is a paramount challenge to develop radiation-hardened, transparent and super-stable vacuum UV-resistant materials for deep-space missions and satellite deployments.

Stannic dioxide is an N-type wide band gap transparent semiconductor. It is suited to required stability (MP 1630 celsius), strong by high elastic moduli, and resistant to oxidation. It qualifies, primarily, for space-grade optoelectronic applications [2].
Recent development in defect engineering of materials show that transition element doping in the host SnO_2 profoundly alters its electronic structure and radiation behaviour. In particular, doping by Co, 3d-electronic states modulate energy band structure inducing many optical features in UV region [3,4]. These feature so far are less explored for space environment.

This study systematically addresses the space ultraviolet compatibility of synthesized samples of cobalt doped stannic dioxide nanocrystals utilizing UV-Visible absorption spectroscopy. The underlying mechanism of solarization resistance and lattice stabilization by cobalt incorporation positions the materials as a robust, radiation hardened matrix suitable for next generation deep-space optical windows and protective coatings [5].

2. Materials and method

It can be synthesized by various methods such as spray pyrolysis or flame spray synthesis [6,7], laser removal process [8], mini arc plasma [9], hydrothermal [10,11], amorphous citrate route [12], wet chemical method [13], solid-state reaction [14], sol-gel [15,16], co-precipitation [17], and others. Microstructural quantum confinement in particles of sizes less than 10 nm is usually observed [18, 19]. We used facile coprecipitation method for synthesis.

Analytic grade chemicals were procured from Sigma Aldrich, Alfci Aser and Rankem, and used directly for preparation of dilute doped stannic dioxide $Sn_{1-x}Co_xO_2$, x= 0.08. In a process, 2.379 x g of hexahydrate cobalt chloride was dissolved in deionized water at room temperature to make 100 ml solution, and 3.506(1-x) g of pentahydrate stannic chloride was dissolved in deionized water to make 100 ml solution. The two solutions were mixed and magnetically stirred. The pH of the solution was maintained to 8 by means of dropwise addition of aqueous ammonia under continuous stirring by magnetic stirrer for 3 hours at room temperature when precipitate was formed. The precipitate was centrifuged and rinsed with deionized water several times. The obtained precipitate was dried in oven at 120°C for 5 hours to get powder of the oxide.

3. Results and Discussion

XRD studies for crystalline phase

The x-ray diffractions by samples show wide bases of peaks in their diffractograms of Figure 1, whose origin is believed to be instrumental broadening and broadening due to nanometric crystallites in the samples. One is aware of Bragg's law for the strong intensity of x-rays after diffraction by atoms in the family of planes (h k l) in usual notations:

$$2\, d_{hkl} \sin \theta_{hkl} = \lambda \quad (1)$$

Impurity effect on peak position is that it shifts on increasing impurity percentage. This may be attributed to dopant-size-induced microstrain in ambient unit cells. The ionic size of Co is 74.5 pm in oxidation state +2 and 61 pm in +3 state, whereas host size in +4 oxidation state is 83 pm.

The (h k l) plane in the tetragonal crystal system to which the patterns belong, the Bragg spacing is given by

$$\frac{1}{d_{hkl}^2} = \frac{(h^2+k^2)}{a^2} + \frac{l^2}{c^2} \quad (2)$$

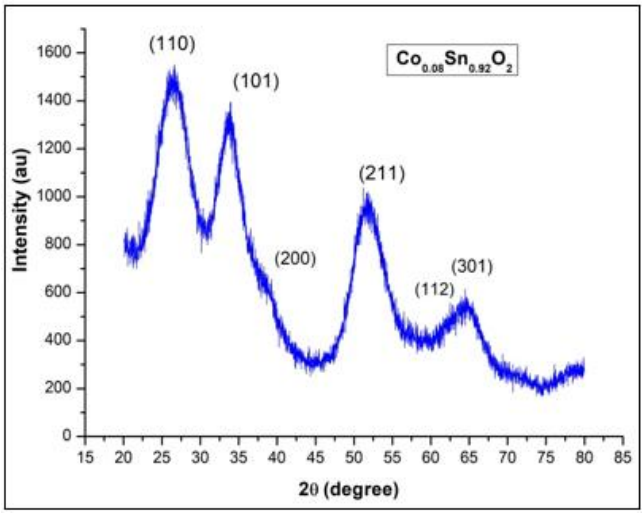

Figure 1: XRD pattern of the sample

The lattice parameters for the samples are found using the x-ray pattern. For (110), *a* is 1.414 d. These are consistent with JCPDS data file no. 41-1445, rutile (tetragonal) structure of symmetry space group P4 2/mnm. with lattice parameters *a*=0.47 nm and c=0.32 nm. Other characterizations also suggested the same crystalline parameters.

UV-Visible spectroscopy

The main part of the work was to study the sample for radiation response, especially in space ultraviolet region. For this, a radiation wavelength 800nm to 200nm was incident on cuvette containing the sample in the UV-Visible spectrometer. Particular attention was given to the ultraviolet region because of its relevance to materials intended for **UV** absorption, attenuation, shielding, and space-related optical applications.

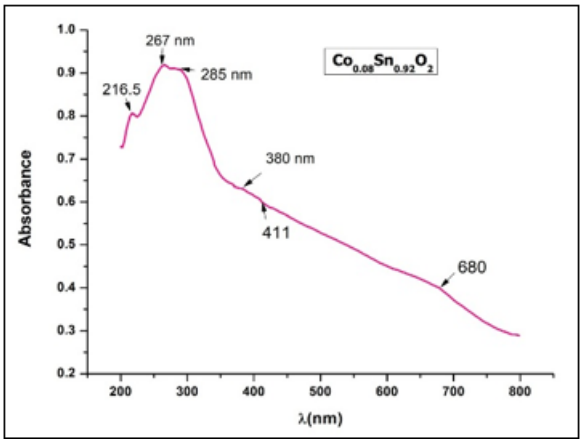

Figure 2: Absorbance spectrum of the sample

Figure 2 shows how the absorbance depended on the wavelength. Peak absorbance covers mainly UV region. The absorption is predominantly observed in the ultraviolet (UV) region, indicating a strong interaction of the sample with high-energy UV photons. The relatively low absorption in the visible region suggests comparatively higher optical transparency in the visible range. The observed UV absorption may be associated with electronic transitions from the valence band to the conduction band and/or transitions involving defect or localized states, depending on material's electronic structure.

The position of the absorption edge is particularly important because it can be used to estimate the optical band gap. A sudden rise in absorption observed near band edge in UV-region can be used to estimate optical BG; the appropriate Tauc relation, depending on whether the transition is direct or indirect, gives the optical band gap. If defect or localized states are present within the forbidden gap, they may also contribute to sub-band-gap absorption and modify the shape of the absorption edge.

The predominance of UV absorption together with comparatively weak absorption in the visible region suggests that the material may possess useful UV-selective optical characteristics. Such behaviour is of interest for UV filtering, UV shielding, photodetection, and other optoelectronic applications.

The wavelength-dependent optical constants of the sample were further evaluated from the experimental spectral data. Figures 3 illustrate the variation of the refractive index (n), real part of the dielectric constant (ε_1), imaginary part of the dielectric constant (ε_2), and extinction coefficient (k).

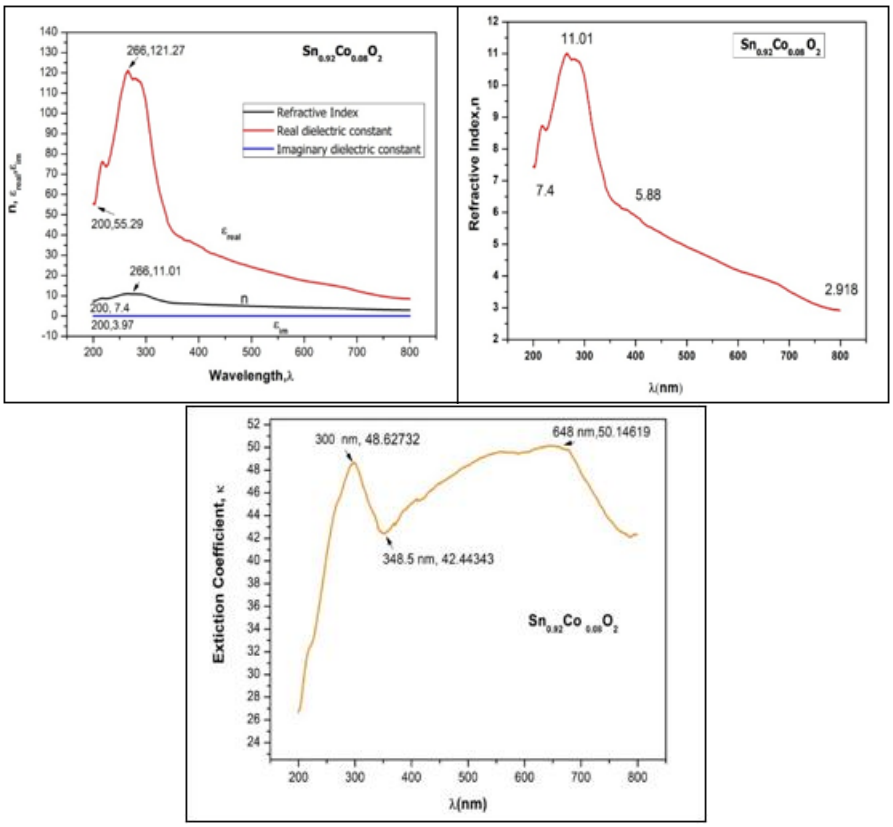

Figure 3: Refractive index, real and imaginary dielectric constant, and extinction coefficient

The refractive index exhibits appreciable wavelength dependence, particularly in the UV region. This behaviour indicates significant optical dispersion, arising from the interaction of the electromagnetic field with the electronic polarization of the material. The enhanced dispersion near the absorption region is expected because the optical response becomes strongly influenced by electronic transitions when the photon energy approaches characteristic transition energies of the material. Since the phase speed of electromagnetic radiation in a non-magnetic medium is, approximately,

$$v_p = \frac{c}{n}$$

An increase in refractive index n corresponds to a decrease in phase speed relative to its value in vacuum. Therefore, the result may be described as reduced phase speed of UV radiation inside the material.

The real part of the dielectric function, ε_{real}, represents the dispersive or polarization component of the optical response, whereas the imaginary part, ε_{im}, is associated primarily with optical absorption and energy dissipation. Thus, the simultaneous variation of $\varepsilon_{real}$and ε_{im}in the UV region indicates enhanced interaction between the incident radiation and the electronic system of the sample.

The extinction coefficient $k$describes the attenuation of electromagnetic radiation within the material. Its enhancement in the UV region is consistent with the strong absorption observed in Figure 2. Therefore, the variation of n, κ, ε_{real}, and ε_{im} collectively confirms that the strongest optical interaction of the sample occurs in the UV spectral region.

Optical density and UV absorption

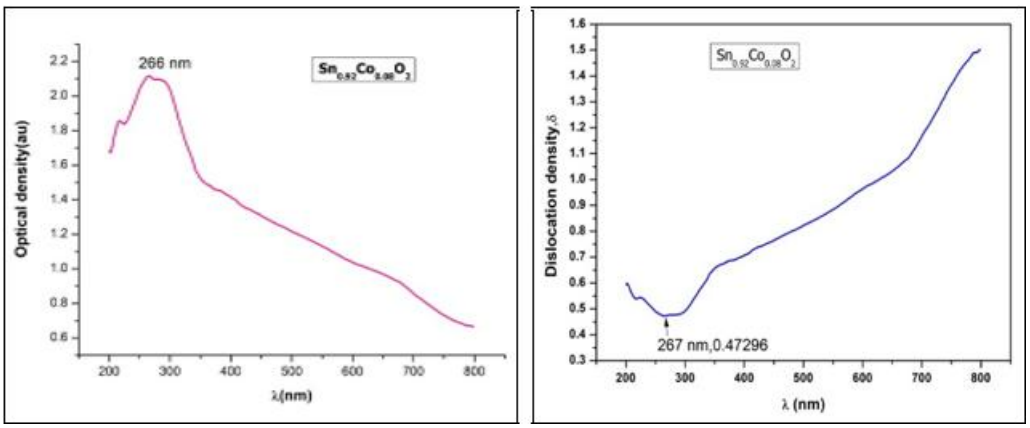

Figure 4: High optical density and low dislocation density in UV region

The optical density in Figure 4 exhibits pronounced behaviour in the UV region. The enhanced optical density is consistent with the increased absorbance observed in Figure 2 and indicates strong attenuation of incident UV radiation by the sample.

The combined observation of high absorbance, high optical density, and enhanced extinction response in the UV region demonstrates that the sample is particularly effective for applications requiring UV attenuation or selective UV absorption, including UV-shielding coatings, optical filters, photodetectors, radiation-protection materials, and selected space-related optical components.

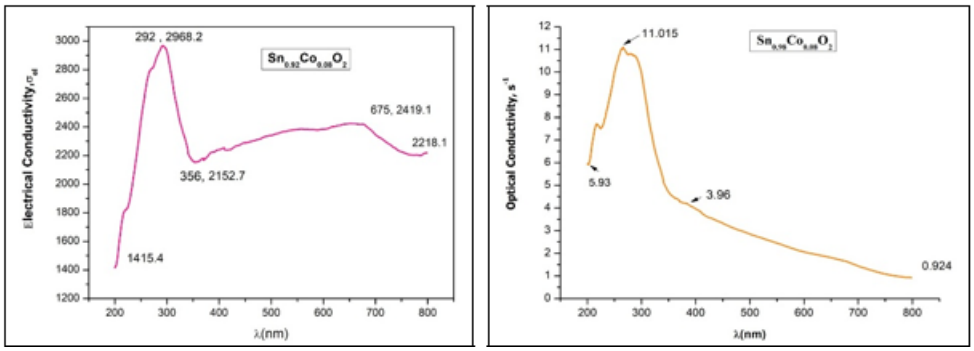

Figure 5: Electrical and optical conductivities in UV region

An increase in optical conductivity in the UV region indicates enhanced excitation and transport of charge carriers under high-energy photon irradiation. This behaviour is consistent with the strong absorption observed near the fundamental absorption edge, where incident photons possess sufficient energy to promote electronic transitions.

If the electrical conductivity increases with frequency, the behaviour may indicate a frequency-dependent charge-transport mechanism involving localized charge carriers, defect states, hopping processes, grain boundaries, or interfacial polarization. In nanostructured or defect-containing materials, such mechanisms can contribute significantly to the high-frequency response.

The correlation between optical absorption, dielectric response, and conductivity is particularly important. Enhanced UV absorption can generate photoexcited carriers, while the resulting carrier dynamics influence the complex dielectric function and optical conductivity. Thus, the observed UV response is not an isolated optical phenomenon but reflects the coupled electronic, dielectric, and conductive behaviour of the material.

4. Conclusion

The sample of cobalt doped stannic dioxide nanocrystal was synthesized, characterized, and investigated for radiation resistance in space. The UV–Visible spectroscopic investigation demonstrated a pronounced and selective optical response in the ultraviolet region of 200–800 nm. The absorption spectrum shows strong UV absorption accompanied by a comparatively lower absorbance in the visible region, indicating preferential interaction of the material with high-energy UV photons. A sharp increase in absorption near the UV absorption edge suggests the onset of significant electronic transitions and provides an important basis for evaluating the optical band gap.

The wavelength-dependent variation of the refractive index, extinction coefficient, and complex dielectric constants further confirms the strong optical dispersion and enhanced interaction of the sample in the UV region. The increase in optical density and extinction response is consistent with the observed strong UV absorption and indicates effective attenuation of UV radiation.

The conductivity response provides additional evidence of the interaction between incident radiation and charge carriers in the material. The enhanced optical/electrical response at higher photon energies or frequencies can be associated with electronic excitation and frequency-dependent charge-transport mechanisms involving localized states and defects.

Overall, the strong UV absorption, significant optical dispersion, enhanced dielectric response, and appreciable conductivity in the high-energy region make the material potentially attractive for UV-shielding, UV filtering, photodetection, optoelectronic, and radiation-management applications. Though suitable for space-related applications, further real-space studies involving UV exposure stability, thermal cycling, vacuum stability, and radiation durability would be necessary in actual space conditions.

Acknowledgement
The author acknowledges for the academic directions, Centre for Nanoscience and Nanotechnology, AN College, BN College, College of Commerce, Arts and Science, Dept of Electrical Engineering, and for the inspiration School of Astronomy, AKU, Patna, India. The article is meant for research awareness.

References

[1] Barth, J. A., Xapsos, M.A. (2021). Space Radiation Environments and Effects on optoelectronic materials and space craft systems. *IEEE Transactions on Nuclear Science,68* (5), 780-795.
[2] Granqvist, C.G. (2007). Transparent conductive electrodes for electrochromic devices: A review. *Solar Energy Materials and Solar Cells,* 91(17), 1529-1554.
[3] Chaudhary, B., Chaudhary, A. (2013). Structural, optical and magnetic properties of Co doped SnO_2

nanoparticles. *Journal of Magnetism and Magnetic Materials,* 337, 36-42.

[4] Gu, F., Wang, S.F., Lü, M. K., Zhou, G.J., Xu, D., Yuan, D.R. (2004). Structure and photoluminescence, properties of Co-doped SnO_2 nanocrystals. *Journal of Physical Chemistry B,* 108(24), 8119-8123

[5] Reddy, K.M., Apparao, B., Space-grade oxide Team. Radiation hardening mechanisms in nanostructured metal oxides under simulated cosmic UV rays. *Materials Today Communications,* 38, 107-115.

[6] Liu W and H Wang, *Journal of Materiomics*, 6, 385-96(2020)

[7] T Sahm, L Madler, A Gurlo, N Barsan, S E Pratsinis, and U. Weimar, *Sens. Actuators B*, 81,165-169 (2004)

[8] F Paraguay-Delgado, W Antunez-Flores, M Miki-Yoshida, A Anguilar-Elguezabal, P Santiago, R Diaz and J A Ascencio, *Nanotechnology*,16 688 (2005).

[9] G Lu, K L Huebner, L E Ocola, M G Josifovska, and J Chen, *J. Nanomaterials*, 1-7(2006)

[10] S Fujihara, T. Maeda, H Ohgi, E Hosono, H. Imai, and S H Kim, *A Chem. Society*, 20, 6476-6481(2004)

[11] F Shaikh et al, *Powder Technol*. 326, 479-87 (2018)

[12] M Bhagwat, P. Shah, V. Ramaswamy, *Materials Letters*.57, 1604-1611(2003)

[13] S Gnanam and V Rajendran, *Digest Journal of Nanomaterials and Biostructures*, 5, 699-704(2010)

[14] F. Li, J. Xu, X. Yu, L Chen, J. Zhu, Z. Yang and X. Xin, *Sens. Actuators B*, 81, 165-169 (2002)

[15] L.L. Hench and J K West, *Chem. Rev.,* 90, 33-72(1990)

[16] L P Wang et al, *Adv. Mater*. 29, 1603286 (2017)

[17] G. Lu et al, *Sens. Actuators B: Chemical* 162, 82-8(2012)

[18] Rohit Raj, N. Kumari, Monalisa, BC Rai, NA Karimi, R K Singh, N Kumar, *Materials Today: Proceedings*, 66(4), 1750-55 (2022)

[19] Nitu Kumari, R Raj, Monalisa, N Kumar, B C Rai, *Materials Today: Proceedings*, 65(8), 3573-80 (2022)